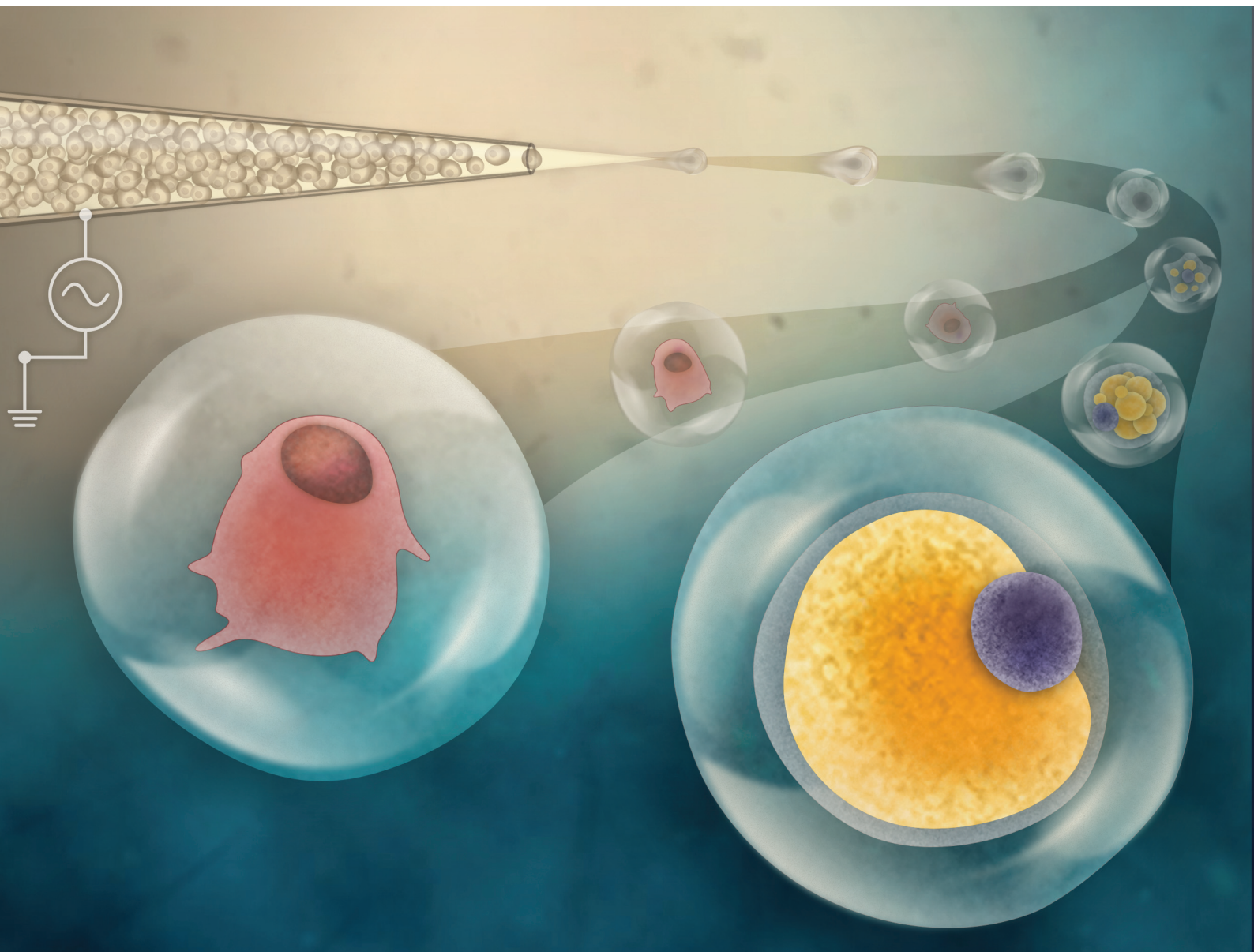


# Biomaterials Science

[rsc.li/biomaterials-science](https://rsc.li/biomaterials-science)



ISSN 2047-4849

## COMMUNICATION



Cite this: *Biomater. Sci.*, 2021, **9**, 3284

Received 12th December 2020,  
Accepted 7th March 2021

DOI: 10.1039/d0bm02100h

rsc.li/biomaterials-science

## Conformal single cell hydrogel coating with electrically induced tip streaming of an AC cone†

Zehao Pan,‡<sup>a</sup> Loan Bui,‡<sup>b</sup> Vivek Yadav,‡<sup>a</sup> Fei Fan,<sup>b</sup> Hsueh-Chia Chang  \*<sup>a,b,c</sup> and Donny Hanjaya-Putra  \*<sup>a,b,c</sup>

Encapsulation of single cells in a thin hydrogel provides a more precise control of stem cell niches and better molecular transport. Despite the recent advances in microfluidic technologies to allow encapsulation of single cells, existing methods rely on special crosslinking agents that are pre-coated on the cell surface and subject to the variation of the cell membrane, which limits their widespread adoption. This work reports a high-throughput single-cell encapsulation method based on the “tip streaming” mode of alternating current (AC) electrospray, with encapsulation efficiencies over 80% after tuned centrifugation. Dripping with multiple cells is curtailed due to gating by the sharp conic meniscus of the tip streaming mode that only allows one cell to be ejected at a time. Moreover, the method can be universally applied to both natural and synthetic hydrogels, as well as various cell types, including human multipotent mesenchymal stromal cells (hMSCs). Encapsulated hMSCs maintain good cell viability over an extended culture period and exhibit robust differentiation potential into osteoblasts and adipocytes. Collectively, electrically induced tip streaming enables high-throughput encapsulation of single cells with high efficiency and universality, which is applicable for various applications in cell therapy, pharmacokinetic studies, and regenerative medicine.

## Introduction

Single cell encapsulation in a micrometer-thick microgel is a new protective bioengineering strategy to increase the surface-to-volume ratio in cell encapsulation for cell therapy, 3D cell culture pharmacokinetic studies, and tissue engineering.<sup>1–3</sup>

Unlike the conventional approach where multiple cells are encapsulated in millimeter sized gel particles, the thin microgel approach improves molecular transport and manipulability, which results in high survival and cell retention *in vivo*.<sup>4–7</sup> Thin microgels or conformal coatings not only allow rapid diffusion of oxygen, nutrients, and cellular waste, but also block immunoglobulins to mitigate innate immune response.<sup>4,8</sup> Moreover, the length scale of single cell laden microgels also helps to avoid several unwanted outcomes including cell hypoxia, fibrotic capsule formation or infarction after transplantation.<sup>9,10</sup>

To achieve single cell encapsulation in a thin microgel, droplet microfluidics, vibrating jets, and inkjet technologies have to compromise between high throughput and the microgel size.<sup>11–14</sup> Despite the recent progress in droplet microfluidics for generating uniform micrometer-sized hydrogel droplets,<sup>15–17</sup> regular PDMS based microfluidic channels often cannot bear the high pumping pressure required to produce droplets similar to the size of the cell using a viscous hydrogel solution. This problem has recently been solved by pre-coating the cells with crosslinking agents (*e.g.* calcium carbonate nanoparticles) or using special crosslinking chemistry.<sup>10,18</sup> The controlled supply of crosslinking agents allows the sol–gel transition to happen within only a few micrometers around the cell, thus automatically eliminating the excess hydrogel around the cell and empty gel particles during extraction into the aqueous phase.<sup>10</sup> However, the adsorption rate of nanoparticles is highly influenced by the “stickiness” of the cell membrane, making the method subject to variation among different cell types and limiting the type of gels that can be used for cell encapsulation. An alternative approach is to use the hydrodynamic method to create a jet thinner than the cell diameter so that Rayleigh instability will be induced around the cell forming a droplet containing a single cell with a thin gel layer.<sup>15</sup> Nonetheless, tuning of both the continuous and dispersed phase flow rates of the flow-focusing design is difficult and hence single-cell occupancy is difficult to achieve. Therefore, there is a need for a new technology that can

<sup>a</sup>Department of Chemical and Biomolecular Engineering, University of Notre Dame, IN 46556, USA. E-mail: hchang@nd.edu, dputra1@nd.edu

<sup>b</sup>Department of Aerospace and Mechanical Engineering, Bioengineering Graduate Program, University of Notre Dame, IN 46556, USA

<sup>c</sup>Harper Cancer Research Institute, University of Notre Dame, IN 46556, USA

† Electronic supplementary information (ESI) available. See DOI: 10.1039/d0bm02100h

‡ These authors contributed equally to this work.

produce robust conformal coating of a single cell with high reproducibility and universality. Ideally, this generic technology does not require the assistance of a high-shear flow and does not depend on the cell and hydrogel-specific adsorbing crosslinking agents.

In this work, we propose a novel method for single cell encapsulation using an immersed alternating current (AC) electrospray that can not only produce predominantly single-cell thin-layered hydrogel beads, but also circumvent the cell- and hydrogel-specific adsorbing crosslinking agents. We demonstrate the universality of the method using both natural (alginate and collagen) and synthetic (hyaluronic acid functionalized with norbornene groups, NorHA) hydrogels as the encapsulation material. Alginate can be crosslinked using divalent cations (*e.g.*,  $\text{Ca}^{2+}$  or  $\text{Mg}^{2+}$ ), while collagen at neutral pH can be crosslinked simply by raising the temperature to 37 °C.<sup>19,20</sup> On the other hand, synthetic NorHA hydrogels can be crosslinked using light-mediated thiol-norbornene chemistry.<sup>21,22</sup> To further demonstrate the universality of the technology across different cell types, the breast cancer cell line MDA-MB-231 and human multipotent mesenchymal stromal cells (hMSCs) are used in all experiments as the model cell lines.

## Experimental

### Electrospray setup

The experiment uses a laser-pulled glass micropipette with a tip diameter of 30  $\mu\text{m}$  (purchased from WPI, FL) and is described previously.<sup>23,24</sup> Briefly, the micropipette was housed in a plastic reservoir through a hole on its side wall (Fig. 1A). The reservoir was attached on a glass substrate with an indium tin oxide (ITO) layer (25 × 75 mm, SPI supplies, USA), which served as the counter electrode in the electrical system and was grounded. The alternating electric potential was generated

from a function generator (Agilent) and amplified by a step-up transformer (Industrial Test Equipment, Port Washington, NY). The output potential was applied through an electrode inside the micropipette that is also in contact with the dispersed phase. All voltages mentioned in this report represent the root mean square voltage. A pressure regulator is used to control the pumping pressure on the aqueous phase. Images and videos were taken with a CCD camera (Retiga EXi, QImaging) connected to an inverted microscope.

### Cell culture

Human breast cancer cells MDA-MB-231 were obtained from ATCC (HTB-26). Cells were thawed and expanded *via* serial passages. Cells were maintained at 37 °C and 5%  $\text{CO}_2$  in DMEM (Cellgro, Corning) supplemented with 10% fetal bovine serum and 1% antibiotics (penicillin and streptomycin).

Human multipotent mesenchymal stromal cells (hMSCs) from the bone marrow were obtained from PromoCell (C-12974). Cells were thawed and expanded *via* serial passages. The cells were grown and maintained in complete mesenchymal growth medium-2 (PromoCell, C-28009) with additional 1% antibiotics (penicillin and streptomycin) at 37 °C and 5%  $\text{CO}_2$ . Cells used for all experiments were between passages 4 and 7.

To induce osteogenic and adipogenic differentiation, hMSCs were switched to MSC osteogenic differentiation medium (PromoCell, C-28013) and MSC adipogenic differentiation medium 2 (PromoCell, C-28016), respectively. The cells were incubated in differentiation media for 7 days. All cell lines were routinely tested for mycoplasma contamination and were negative throughout this study.

### Preparation of suspended cells

Cell suspension preparation for encapsulation was conducted based on the standard procedure.<sup>25</sup> Briefly, to obtain sus-

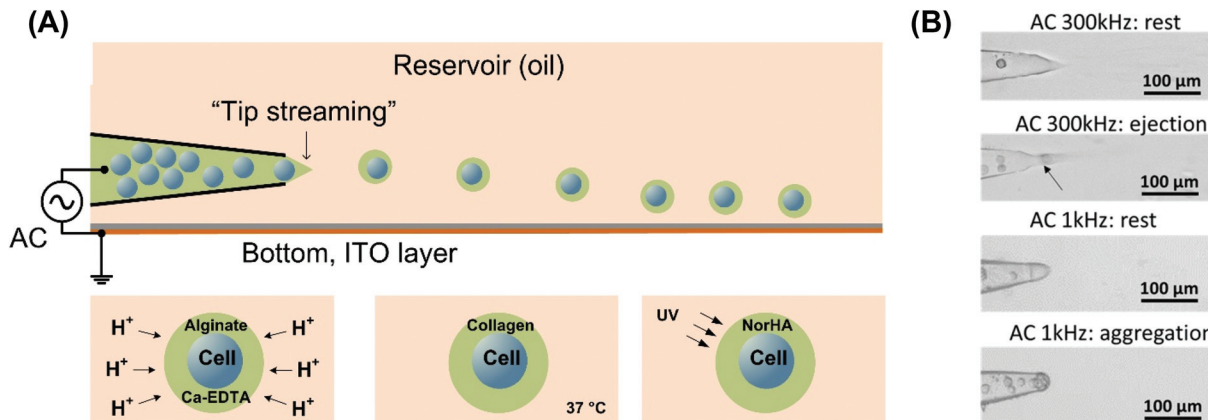


**Fig. 1** (A) Schematic for single-cell gel coating using the tip-streaming mode. For encapsulation with alginate gel, the alginate solution is cross-linked by releasing the premixed Ca-EDTA complex using acetic acid. For encapsulation with collagen gel, the droplets were incubated at 37 °C for 30 minutes to induce gelation. Encapsulation of the NorHA hydrogel was performed by photo-crosslinking of the NorHA precursor solution with UV exposure (10 mW  $\text{cm}^{-2}$ , 365 nm). (B) Snapshots of an MDA-MB-231 cell being ejected through "tip streaming" in alginate solution at high (300 kHz) and low (1 kHz) frequencies.

pended cells, adherent cells were detached using trypsin/EDTA (PromoCell, C-41020) for 5 min.

Centrifugation was performed (300g, 5 min) to remove the trypsin-containing supernatant and to pellet the cells. Cells were then resuspended in PBS at a high concentration (1–2 million cells per ml). Prior to spraying, dispersed individual cells were achieved by pipetting the cell suspension multiple times followed by filtering it through a 40 µm mesh strainer.

### Cell viability

Viable cells were visualized by staining the nuclei with 10 µg ml<sup>-1</sup> Hoechst 3342 (Invitrogen™, H3570) and the cell membrane with 2 µM calcein AM dye for 20 min at room temperature. Dead cells were determined as stained with 4 µM ethidium homodimer-1 (Invitrogen™, L3224) for 30 min at room temperature. Cell viability was quantified using fluorescence microscopy and ImageJ.

### Quantification of differentiated cells

Osteogenic differentiation was detected by staining the cells with Alizarin Red S for extracellular calcium deposits. A 2% Alizarin Red S solution (Sigma-Aldrich, A5533) was prepared in dH<sub>2</sub>O and then filtered to remove the debris. The solution pH of 4.1–4.3 was adjusted with hydrochloric acid or ammonium hydroxide. The cells were washed with PBS and then fixed with 95% methanol for 10 min and washed again with dH<sub>2</sub>O. Staining was performed by incubating the cells with the Alizarin Red S solution for 30 min. After that, the cells were rinsed with dH<sub>2</sub>O and kept in dH<sub>2</sub>O for immediate imaging. The percentage of differentiated cells was calculated and compared between the adherent cells and encapsulated cells. For further quantification of calcium deposits and comparison between control cells and differentiated cells, the absorbance at 520 nm of each well was measured.

Adipogenic differentiation results in the formation of lipid droplets within the cells, which could be identified by staining with Oil Red O solution (BioVision, K580-24) following the protocol suggested by the manufacturer. Briefly the cells were washed with PBS and fixed with 10% formalin for 30 min. The fixed cells were then stained with Oil Red O solution and the cell nuclei could be counterstained with hematoxylin. After staining, the lipid droplets appeared in red color in microscopy images. Finally, the Oil Red O stain can be extracted with isopropanol and the resulting solutions could be quantified by reading the absorbance at 492 nm.

### Encapsulation experiment

Alginate crosslinking was induced using the Ca–EDTA complex to deliver the calcium ion for gelation.<sup>26</sup> The Ca–EDTA complex was made by mixing equal molar solutions of calcium chloride and ethylenediaminetetraacetic acid (EDTA) in HEPES-buffered DMEM (Sigma-Aldrich) solution at pH 7.4. 2% w/w Alginate (300 kDa, low viscosity, Sigma) was then added into the solution and fully dissolved. Cells were added to the mixed solution before electrospray at a final concentration of  $5 \times 10^7$  cells per ml. Crosslinking of the gel coating was achieved by adding a

final concentration of 0.01% acetic acid (Sigma) to the oil phase for 2 minutes. The cells were extracted to cell media through centrifugation after adding 10% w/w 1H,1H,2H,2H-perfluorooctanol (PFO). Staining of alginate was achieved by substituting FITC-labeled alginate (Creative PEGWorks, NC) for 20% of the original alginate solution.

Collagen I (Corning®, 354249) was first neutralized with 100 mM HEPES (pH 7.3 in 2× PBS) before mixing with cells at a final concentration of 2.5 mg ml<sup>-1</sup>. Staining of collagen was achieved by incubating with NHS-FITC (5/6-carboxyfluorescein succinimidyl ester, ThermoFisher) on ice for two hours according to manufacturer's instruction. To prevent premature gelation of collagen, all the preparation and encapsulation steps were performed with cooling using ice. Crosslinking of collagen was achieved by incubating the water-in-oil emulsion at 37 °C for 30 minutes.

NorHA was synthesized using an established protocol.<sup>21,22</sup> NorHA gels were prepared by mixing NorHA macromer (1.2% w/v) with dithiothreitol (DTT) at 0.8 ratio in PBS. The water soluble photoinitiator lithium phenyl-2,4,6-trimethylbenzoylphosphinate (LAP) was used at 0.2% (w/v) unless otherwise stated and was purchased from Sigma-Aldrich. After collecting the cell laden microgel droplets in a microcentrifuge tube, OmniCure® Series 1500 was used for crosslinking the NorHA precursor solution for 5 seconds with UV exposure (10 mW cm<sup>-2</sup>, 365 nm). To visualize the gel layer, 2 mM rhodamine-thiol dye (Kerafast, Boston, MA) was incorporated into NorHA using light-mediated thiol-norbornene chemistry.<sup>22</sup> The cells were extracted to cell media through centrifugation using 25% w/w 1H,1H,2H,2H-perfluorodecanol (PFD).

All extractions were performed in a centrifuge at 200g for 3 minutes. The continuous phase consists of 1% w/w biocompatible fluorosurfactant (RAN Biotechnology, MA) in fluorinated oil (3 M Novec Engineering HFE7500).

### Rheological measurement

NorHA gels precursor solution containing 1.2% (w/v) NorHA, dithiothreitol (DTT, 0.8 ratio), and 0.2% (w/v) water soluble photoinitiator LAP was transferred to syringes with their tips removed, covered with a coverslip, and irradiated with UV light (10 mW cm<sup>-2</sup>, 365 nm) for 5 seconds. NorHA gels were incubated with PBS overnight before mechanical testing. The mechanical properties of the hydrogels were tested using a TA Instruments Discovery HR-2 rheometer. Oscillatory time sweeps were performed on three samples ( $n = 3$ ) at a strain of 0.64% and a frequency of 1 Hz to measure the storage modulus ( $G'$ ) and loss modulus ( $G''$ ). The Young's modulus (substrate elasticity) was calculated following  $E = 2G'(1 + \nu)$  using an average Poisson's ratio ( $\nu$ ) of 0.5.<sup>27,28</sup>

## Results and discussion

### "Tip streaming" mode of AC electrospray

With the appropriate back pressure and a DC (direct current) electric potential applied across a liquid interface, the inter-

face becomes charged and forms a sharp conic structure with a 49 degree half angle (Taylor cone).<sup>29</sup> Despite the earlier attempts to exploit the sharp conic structure to encapsulate cells,<sup>30–32</sup> multiple cells are encapsulated in a single droplet, which is often attributed to recirculation within the Taylor cone.<sup>33</sup> However, a recent discovery in our lab shows that an AC field can produce a much sharper cone (11 degrees) due to dielectric polarization, rather than the direct ion charging of the DC cone.<sup>34</sup> This slender AC cone cannot sustain a recirculation flow and ejects electroneutral droplets much larger than the charged droplets of the DC Taylor cone. Following our earlier jargon,<sup>23</sup> we define such droplet generation from the AC cone as “tip streaming” (Fig. 1A). Stable AC cone and tip streaming only occurs at frequencies beyond the inverse charge relaxation time of the orifice  $D/\lambda R \sim 10$  kHz, where  $D$  is the diffusivity of the dominant ion such as calcium ( $\sim 10^{-5}$  cm $^2$  s $^{-1}$ ),  $\lambda$  is the Debye length of the cell solution ( $\sim$ few nm for the typical cell medium in the dispersed phase) and  $R \sim 20$  microns is the orifice radius. The choice of the frequency should also avoid field penetration into the cell beyond megahertz.<sup>35</sup> Here, we report the first successful encapsulation of the cells with the tip streaming mode of the AC cone at an alternating frequency of 300 kHz.

Consistent with our previous observations, at low frequencies below the inverse charge relaxation time of 10 kHz, a DC Taylor cone is still observed.<sup>36,37</sup> An incoming cell often fails to block the flow supplying the tip streaming and starts to recirculate within the conic area until enough cells aggregate at the tip. The aggregated cells are eventually ejected collectively in a single droplet, as shown in Fig. 1B. This multi-cell encapsulation phenomenon is consistent with earlier findings with DC sprays.<sup>31,38</sup> The broad Taylor cone at low frequencies evolves into the slender AC cone at frequencies higher than the inverse charge relaxation time<sup>34</sup> and each cell is packed into a cone apex without recirculating (Fig. 1B and Movie S1†). Since the tip of the AC cone has a diameter much smaller than the cell, the flow is essentially blocked by this cell at the cone apex and the trailing cells can no longer advance. The apex then pinches off to generate a droplet containing a single cell, while multiple cells may exist in the trailing conic region. There is hence a gating action much like a ball check valve in a funnel.

### Conformal single-cell hydrogel coating

In order to minimize the effect of the electric field on the cells, we chose the voltage potential at the lower end for tip streaming which is found to be around 420 V for 300 kHz. The appropriate applied pressure is chosen to ensure both the formation of the streaming cone and a high flow rate. It is found that when the applied pressure is higher than a critical pressure of 2.4 kPa, dripping droplets with 30 microns to 40 microns in diameter are created. Therefore, the applied pressure is set slightly below the critical pressure at 1.6–2.2 kPa. During tip streaming, tiny liquid droplets which have a size range between one to ten microns are emitted from the cone apex as shown in Fig. 1B. When no cells are present near

the cone, tip streaming has a flow rate of about 5 nL min $^{-1}$  (estimated based on the cell moving speed in the pipette) for the chosen parameters described above. The cells are emitted at a frequency of  $\sim$ 100 Hz. It is important to note that we did not characterize the droplet generation frequency for the tiny tip streaming droplets as they are often below the diffraction limit.

After dispersing the cells, the hydrogel layer is crosslinked by different methods depending on the hydrogel materials, as shown in Fig. 1A. For crosslinking alginate and collagen gels, we used acetic acid and heat incubation respectively. On the other hand, NorHA precursor solution was crosslinked using irradiation with ultraviolet (UV) light (10 mW cm $^{-2}$ , 365 nm) for 5 seconds.<sup>21,39</sup> In order to ensure that the cell is completely encapsulated by the hydrogel layer after the crosslinking process, the emulsion is first placed in an orbital shaker at 1000 rpm for two minutes to drive the cell closer to the center of the droplet without affecting the droplet monodispersity.<sup>18</sup> Immediately after shaking the droplets, the alginate droplets are crosslinked by adding 0.01% v/v acetic acid to the oil for two minutes<sup>26</sup> and the collagen droplets are gelled by incubation at 37 °C for 30 minutes.

Extraction of the droplets into the cell medium is achieved by centrifugation after adding the cell medium to the centrifuge tube containing the emulsion. During extraction, the interfacial tension between the cell medium and the oil phase is reduced using 1H,1H,2H,2H-perfluorooctanol (PFO) for alginate and collagen. Most empty droplets generated from “tip streaming” are more than ten times smaller than the encapsulated single-cell particles in volume; thus, the majority of them can be left in the oil phase by choosing an appropriate concentration of PFO that allows the larger cell-encapsulated beads to cross over the water/oil interface but not the smaller streaming droplets.

### Characterization of the encapsulated cells

Visualization of the microgels was done using FITC-labeled alginate and NHS-FITC dye to label the primary amine group in the collagen gel (Fig. 2A–C). It is found that using a PFO concentration of 10% w/w allows the extraction of most cell-encapsulated alginate and collagen beads but most small empty particles were left behind in the oil phase, as shown in Fig. 2A and B. While keeping the centrifugal force and time the same, a significant amount of empty alginate gel particles from streaming droplets is extracted using 20% w/w PFO as shown in Fig. 2C and Fig. S1A.† At the same centrifugation force, we demonstrate the sorting of cell loaded droplets by controlling the interfacial tension and increasing the single cell laden droplet percentage from 30% to more than 80% as shown in Fig. 2E and Fig. S1A.† However, it is important to note that 20% w/w PFO was not sufficient to break the interfacial surface tension between the NorHA microgel and the oil (Fig. S1A†). Instead, using 25% of 1H,1H,2H,2H-perfluorodecanol (PFD) allowed the extraction of 81% single cell laden microgel from the water oil emulsion (Fig. 2D and E), whereas using 10% PFD (data not shown) did not allow the extraction

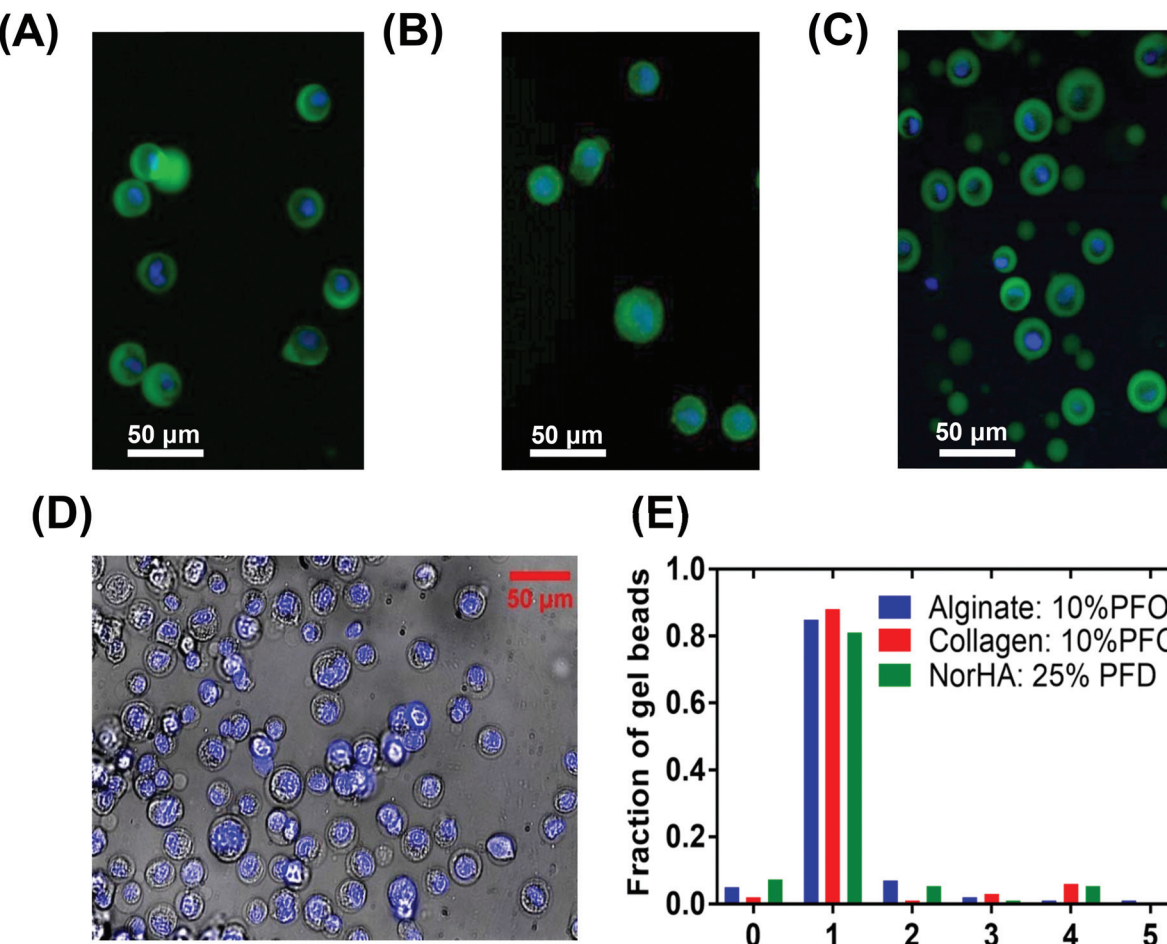


**Fig. 2** (A) MDA-MB-231 cells encapsulated in the alginate gel. Green: alginate gel; blue: cell nucleus. (B) MDA-MB-231 cells encapsulated in collagen gel. Green: collagen gel; blue: cell nucleus. (C) Alginate gel particles extracted using 20% w/w PFO including both empty streaming droplets and encapsulated cells. Green: alginate gel; blue: cell nucleus. (D) MDA-MB-231 cells encapsulated in NorHA microgels extracted using 25% w/w PFD including both empty streaming droplets and encapsulated cells. Blue: cell nucleus. Scale bars: 50 µm. (E) Fraction of encapsulated cells per microgel bead.

of any cell laden microgels from the oil phase. We suspect that the difference in interfacial surface tension allows us to isolate these microgels with different types of perfluorocarbon liquids.

To further characterize the single-cell encapsulated microgels, their morphologies are studied using light and fluorescence microscopy techniques. The representative images of alginate, collagen, and NorHA encapsulated MDA-MB-231 cells are shown in Fig. 3A, C and E respectively. The lighter green area indicates the volume of the cell and the darker green area indicates the hydrogel layer of alginate and collagen gels. NorHA microgels, on the other hand, are modified with thiol-dyes to indicate the hydrogel layer in red and the volume of the cell in green.<sup>21,39</sup>

Thirty randomly chosen single-cell beads are analyzed for each case. For each single-cell bead, the minimum thickness  $t_{\min}$  and the maximum thickness  $t_{\max}$  of the gel layer can be measured as shown by the bars in Fig. 3B, D and F. The average thickness of the hydrogel layer is taken by the average

of  $t_{\min}$  and  $t_{\max}$ . The alginate, collagen and NorHA encapsulated hydrogel beads have the average thickness of  $4.4 \pm 0.8$ ,  $4.1 \pm 2.0$  and  $2.85 \pm 1 \mu\text{m}$ , respectively. To better evaluate how close the cell is placed to the center of the gel bead, concentric index (CI) is defined as

$$\text{CI} = \frac{t_{\max} - t_{\min}}{t_{\max} + t_{\min}}$$

When the cell is placed at the most center of the bead, CI is equal to zero; when the cell is placed at the edge of the bead, CI is equal to one. If an arbitrary value of CI of 0.8 is used to classify the single-cell beads into centered and off-centered groups, more than 86% beads are centered, as shown in Fig. 3B, D and F.

The viability of the MDA-MB-231 cells is studied using the live/dead cell viability assay. Cell viability immediately after microgel encapsulation was  $88.25 \pm 6.63\%$  and  $93.14 \pm 2.65\%$  for alginate and collagen respectively. The viability remained  $82.97 \pm 0.9\%$  and  $73.81 \pm 5.14\%$  after 24 hours *in vitro* for the

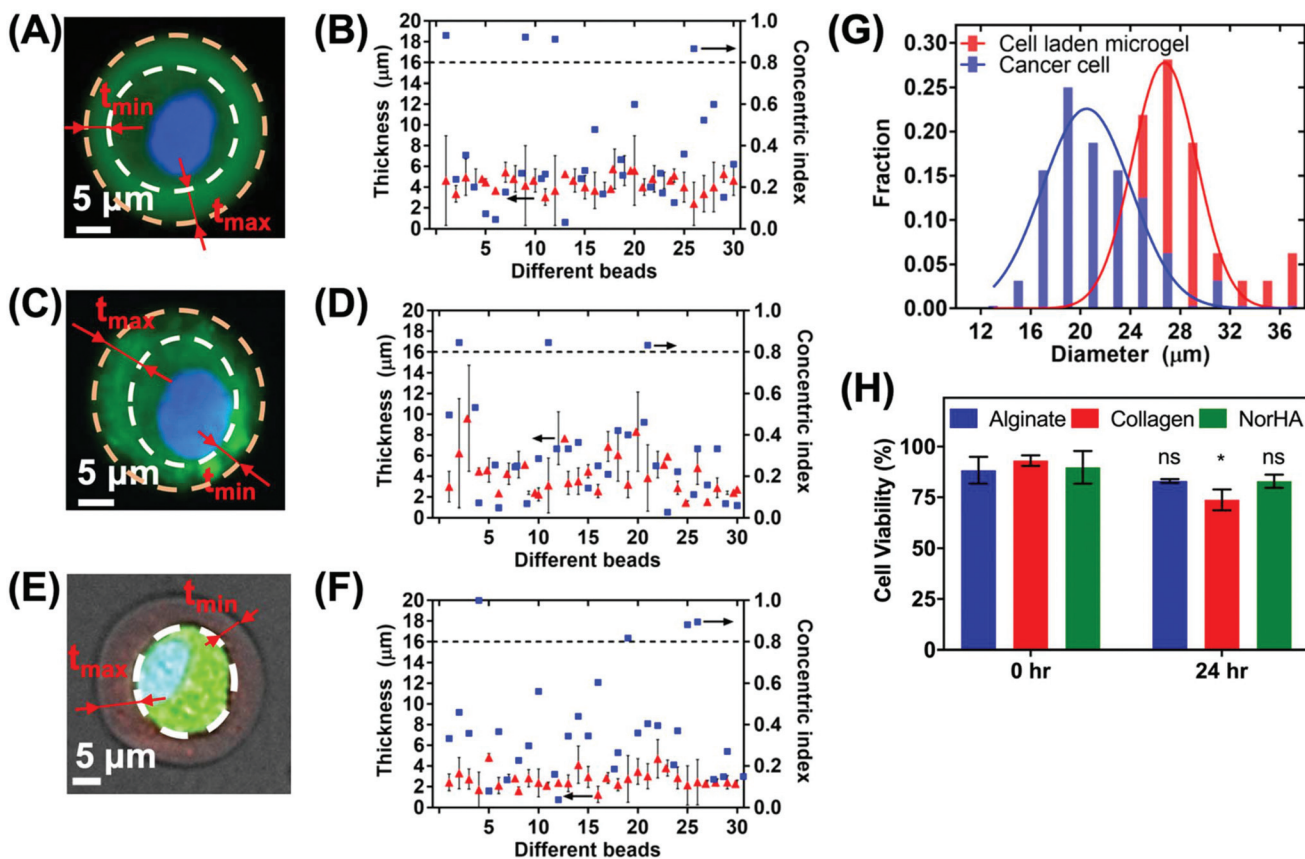


**Fig. 3** (A) Representative image of a MDA-MB-231 cell encapsulated in an alginate gel particle. The cell occupies the middle region of the bead with lighter fluorescence intensity. White dashed lines delineate cell boundaries. (B) Gel layer thickness (red triangle) and concentric index (blue square) of 30 randomly chosen single-cell-encapsulated alginate gel particles. (C) Representative image of a MDA-MB-231 cell encapsulated in a collagen gel particle. (D) Gel layer thickness (red triangle) and concentric index (blue square) of 30 randomly chosen single-cell-encapsulated collagen gel particles. (E) Representative image of a MDA-MB-231 cell encapsulated in a NorHA gel particle. (F) Gel layer thickness (red triangle) and concentric index (blue square) of 30 randomly chosen single-cell-encapsulated NorHA gel particles. (G) Distribution of microgels and cells from (F), depicting conformal coating. (H) Viability of single cells encapsulated in alginate or collagen particles right after encapsulation and after 24 hours. Pair sample *t* test *P*-values = 0.32, 0.028 and 0.15 for alginate, collagen and NorHA encapsulated cells, respectively.

alginate and collagen encapsulated cells respectively. We did not observe cell proliferation within the microgels following cell encapsulation, which is consistent with previous reports using high molecular weight alginate gels.<sup>10</sup> Since the NorHA gel is polymerized using free radical polymerization, the photo-initiator (*e.g.*, LAP) concentration plays an important role in cell viability.<sup>40</sup> The free radicals generated by the UV dosage may affect cell viability, unless they are all consumed in a reaction. A higher LAP concentration leads to faster gelation kinetics, but the excessive free radicals formed cause detrimental effects on cells. The viability of cells immediately after spraying was studied using two photo-initiator concentrations of 0.2% (w/v) and 0.3% (w/v) for the same UV exposure (10 mW cm<sup>-2</sup>, 365 nm, 5 seconds) as shown in Fig. S1B.† The 0.3% (w/v) LAP concentration showed less than 60% cell viability, while 0.2% (w/v) showed more than 84% cell viability immediately after cell encapsulation. The optimized LAP concentration was used to obtain 89.75 ± 8.01% cell viability immediately after encapsulation and more than 80% of the

cells were alive after 24 hours *in vitro* for the NorHA microgel as shown in Fig. 3H.

#### Differentiation potential of the encapsulated hMSCs

Since hyaluronic acid hydrogels have been previously shown to support self-renewal of stem cells, tissue morphogenesis, and angiogenesis,<sup>25,27,28,41–43</sup> we focus our next investigation using NorHA hydrogels to encapsulate hMSCs and to study their differentiation potential. We first encapsulated single hMSCs in a thin layer of the NorHA microgel having an average thickness of 4.0 ± 1.8 μm as shown Fig. 4A and B. Next, we demonstrated that the encapsulated hMSCs remain more than 80% viable for three consecutive days as shown in Fig. 4C. Furthermore, in order to evaluate their differentiation potential, the encapsulated hMSCs were cultured in either osteogenic or adipogenic differentiation medium. For osteogenic differentiation, calcium deposits were detected by Alizarin Red S staining in both adherent and encapsulated cells (cultured in osteogenic differentiation medium), which are significantly

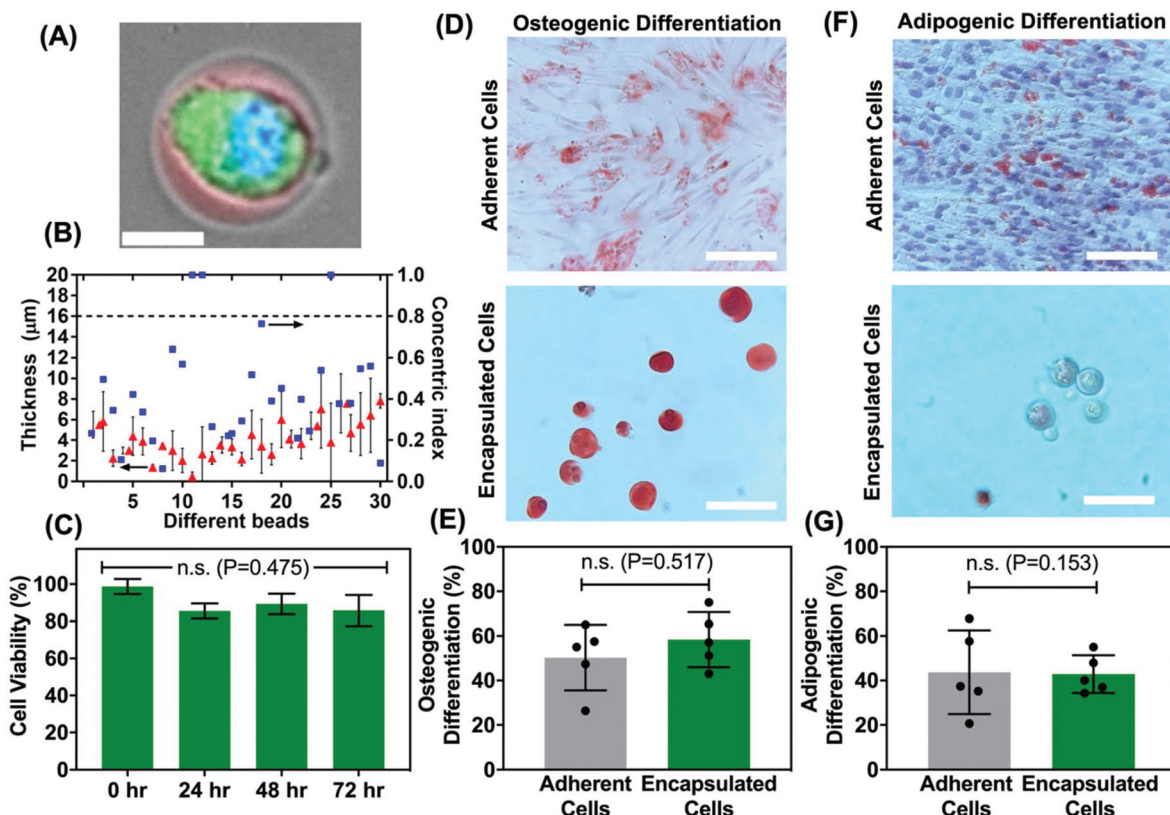


**Fig. 4** Human MSC encapsulation and differentiation within the NorHA microgel. (A) Representative image of hMSCs encapsulated in the NorHA microgel with the fluorescence image superimposed with the bright field image (blue: cell nucleus, green: calcein stain). Scale bar: 20  $\mu$ m. (B) Gel layer thickness (red triangle) and concentric index (blue square) of 30 randomly chosen single hMSC encapsulated NorHA gel particles. (C) Viability of encapsulated cells 1 day, 2 days, and 3 days after encapsulation. Data represent mean  $\pm$  stdev. of five experimental runs. (D) Microscopy images of osteogenic differentiation of hMSCs (adherent and NorHA-encapsulated cells). Differentiated cells, cultured in MSC osteogenic differentiation medium for 7 days, show calcium deposits (bright orange-red, top) as stained with Alizarin Red S solution. Scale bars are 100  $\mu$ m. (E) Quantification graph compares the percentage of positive differentiated encapsulated cells versus adherent cells. P-Value = 0.517. (F) Microscopy images of adipogenic differentiation of hMSCs (adherent and NorHA-encapsulated cells). Differentiated cells, cultured in MSC adipogenic differentiation medium for 7 days, show lipid deposits as stained with Oil Red O solution. Scale bars are 100  $\mu$ m. (G) Quantification graph compares the percentage of positive differentiated encapsulated cells versus adherent cells. P-Value = 0.153. Data represent mean  $\pm$  stdev. of five experimental runs with  $\geq 30$  microgels of cells analysed per condition in each replicate run.

different from control cells maintained in growth medium (Fig. 4D and Fig. S2†). It is important to note that control hMSCs maintained in growth medium do not stain positive for Alizarin Red S, which may suggest that Alizarin Red S does not demonstrate non-specific binding to the NorHA hydrogels (Fig. S2†). More importantly, we did not observe a significant difference in the osteogenic differentiation potential between the encapsulated cells ( $58.34 \pm 12.40\%$ ) and adherent cells ( $50.26 \pm 14.76\%$ ) as shown in Fig. 4E. For adipogenic differentiation, lipid droplets were also detected in both adherent and encapsulated cells, which were cultured in adipogenic differentiation medium as shown in Fig. 4F and Fig. S2.† There is no significant difference in the adipogenic differentiation potential between the adherent and encapsulated cells (Fig. 4G). These observations are consistent with previous studies that suggest that HA hydrogels with a moderate elastic modulus ( $2.86 \pm 0.02$  kPa; Fig. S3†) and cultured in the appropriate

differentiation medium can support the osteogenic and adipogenic differentiation of hMSCs.<sup>20,44,45</sup>

We chose NorHA conditions with fixed rheological and mechanical properties (Fig. S3†) to demonstrate the feasibility of our novel technology to support the viability and differentiation potential of hMSCs. However, this unique technology can be broadly applied to other types of hydrogels with tunable mechanics, through either covalent or physical cross-linking, to enable precise control over stem cell differentiation.<sup>46–48</sup> Moreover, these microgels containing cells can be used as versatile bio-inks for various 3D printing applications,<sup>39,49–51</sup> as well as building blocks for annealed particle hydrogels and granular hydrogels for regenerative medicine.<sup>52–54</sup> Collectively, we show that the encapsulated hMSCs within the NorHA microgel using our novel platform remain in high viability and preserve their robust differentiation potential, which could pave the way for a variety of

applications from fundamental stem cell biology research to developing therapeutic cell-based therapy.

## Conclusions

In conclusion, we demonstrate a single-cell encapsulation method based on immersed AC electrospray that is compatible with traditional crosslinking strategies for both natural and synthetic hydrogels. Using the “tip streaming” mode, cells are ejected as they block the streaming flow of alginate, collagen, or NorHA precursor solution resulting in a hydrogel droplet with a single cell. An alternating frequency higher than the charge relaxation frequency of the precursor solution is shown to be able to generate slender cones that help avoid cell aggregation within the conic meniscus. After crosslinking, the smaller empty particles can be separated from the single-cell particles using moderate extraction conditions resulting in predominant single cell particles in cell media (>80%). The final gel layer around the cell has a typical thickness of around four microns allowing fast nutrient transport and better cell survival. Thanks to the common electrospray behavior that exists in many solution types, we envision that such a technology can be applicable to various cell types and hydrogel systems, such as photo-crosslinked<sup>47,55</sup> and dynamic hydrogels.<sup>46,56,57</sup> Since the microgel fabrication technique can influence the properties of granular hydrogels,<sup>54</sup> this high-throughput single-cell encapsulation technique can be used to generate microgels with tunable properties as building blocks for granular hydrogels.<sup>58</sup> Collectively, this unique technology has the potential to make high impact contribution in a range of applications in cell therapy, pharmacokinetic screening, and regenerative medicine.

## Author contributions

Z.P., L.B., and V.Y. designed and performed research, analyzed data, and wrote the manuscript. F.F. performed research and analyzed hydrogel data. D.H.-P. and H.-C.C. conceived the ideas, designed the experiments, interpreted the data, and wrote the manuscript. All authors have approved the manuscript.

## Conflicts of interest

The authors have declared that no conflict of interest exists.

## Acknowledgements

Z.P., V.Y. and H.-C.C. acknowledge the support of NIH Grant R21-HG009010-01 and the C. Moschetto Discovery Fund. L.B., F.F., and D.H.-P acknowledge the support from the University of Notre Dame through the “Advancing our Vision” initiative, the Harper Cancer Research Institute – American Cancer

Society Institutional Research Grant (IRG-17-182-04), and the Career Development Award (19CDA34630012) from the American Heart Association (AHA).

## Notes and references

- 1 T. Kamperman, M. Karperien, S. Le Gac and J. Leijten, *Trends Biotechnol.*, 2018, **36**, 850–865.
- 2 K. Matula, F. Rivello and W. T. S. Huck, *Adv. Biosyst.*, 2020, **4**, 1900188.
- 3 S. S. Terekhov, I. V. Smirnov, A. V. Stepanova, T. V. Bobik, Y. A. Mokrushina, N. A. Ponomarenko, A. A. Belogurov, M. P. Rubtsova, O. V. Kartseva, M. O. Gomzikova, A. A. Moskovtsev, A. S. Bukatin, M. V. Dubina, E. S. Kostryukova, V. V. Babenko, M. T. Vakhitova, A. I. Manolov, M. V. Malakhova, M. A. Kornienko, A. V. Tyakht, A. A. Vanyushkina, E. N. Ilina, P. Masson, A. G. Gabibov and S. Altman, *Proc. Natl. Acad. Sci. U. S. A.*, 2017, **114**, 2550–2555.
- 4 A. S. Mao, B. Özkale, N. J. Shah, K. H. Vining, T. Descombes, L. Zhang, C. M. Tringides, S.-W. Wong, J.-W. Shin, D. T. Scadden, D. A. Weitz and D. J. Mooney, *Proc. Natl. Acad. Sci. U. S. A.*, 2019, **116**, 15392–15397.
- 5 T. Kamperman, S. Henke, C. W. Visser, M. Karperien and J. Leijten, *Small*, 2017, **13**, 1603711.
- 6 J. M. de Rutte, J. Koh and D. Di Carlo, *Adv. Funct. Mater.*, 2019, **29**, 1900071.
- 7 B. Oh, V. Swaminathan, A. Malkovskiy, S. Santhanam, K. McConnell and P. M. George, *Adv. Sci.*, 2020, **7**, 1902573.
- 8 J. T. Wilson, W. Cui, V. Kozlovskaia, E. Kharlampieva, D. Pan, Z. Qu, V. R. Krishnamurthy, J. Mets, V. Kumar, J. Wen, Y. Song, V. V. Tsukruk and E. L. Chaikof, *J. Am. Chem. Soc.*, 2011, **133**, 7054–7064.
- 9 O. Veiseh, J. C. Doloff, M. Ma, A. J. Vegas, H. H. Tam, A. R. Bader, J. Li, E. Langan, J. Wyckoff, W. S. Loo, S. Jhunjhunwala, A. Chiu, S. Siebert, K. Tang, J. Hollister-Lock, S. Aresta-Dasilva, M. Bochenek, J. Mendoza-Elias, Y. Wang, M. Qi, D. M. Lavin, M. Chen, N. Dholakia, R. Thakrar, I. Lacík, G. C. Weir, J. Oberholzer, D. L. Greiner, R. Langer and D. G. Anderson, *Nat. Mater.*, 2015, **14**, 643.
- 10 A. S. Mao, J.-W. Shin, S. Utech, H. Wang, O. Uzun, W. Li, M. Cooper, Y. Hu, L. Zhang, D. A. Weitz and D. J. Mooney, *Nat. Mater.*, 2016, **16**, 236.
- 11 C. W. Visser, T. Kamperman, L. P. Karbaat, D. Lohse and M. Karperien, *Sci. Adv.*, 2018, **4**, eaao1175.
- 12 T. Xu, H. Kincaid, A. Atala and J. J. Yoo, *J. Manuf. Sci. Eng.*, 2008, **130**, 021017.
- 13 G. Kamalakshakurup and A. P. Lee, *Lab Chip*, 2017, **17**, 4324–4333.
- 14 R. M. Schoeman, E. W. M. Kemna, F. Wolbers and A. van den Berg, *Electrophoresis*, 2014, **35**, 385–392.
- 15 A. A. Tomei, V. Manzoli, C. A. Fraker, J. Giraldo, D. Velluto, M. Najjar, A. Pileggi, R. D. Molano, C. Ricordi, C. L. Stabler

- and J. A. Hubbell, *Proc. Natl. Acad. Sci. U. S. A.*, 2014, **111**, 10514–10519.
- 16 D. M. Headen, J. R. García and A. J. García, *Microsyst. Nanoeng.*, 2018, **4**, 17076.
- 17 M. Dhar, J. N. Lam, T. Walser, S. M. Dubinett, M. B. Rettig and D. Di Carlo, *Proc. Natl. Acad. Sci. U. S. A.*, 2018, **115**, 9986–9991.
- 18 P. S. Lienemann, T. Rossow, A. S. Mao, Q. Vallmajó-Martin, M. Ehrbar and D. J. Mooney, *Lab Chip*, 2017, **17**, 727–737.
- 19 S. Kusuma, Y.-I. Shen, D. Hanjaya-Putra, P. Mali, L. Cheng and S. Gerecht, *Proc. Natl. Acad. Sci. U. S. A.*, 2013, **110**, 12601–12606.
- 20 N. Huebsch, E. Lippens, K. Lee, M. Mehta, S. T. Koshy, M. C. Darnell, R. M. Desai, C. M. Madl, M. Xu, X. Zhao, O. Chaudhuri, C. Verbeke, W. S. Kim, K. Alim, A. Mammoto, D. E. Ingber, G. N. Duda and D. J. Mooney, *Nat. Mater.*, 2015, **14**, 1269–1277.
- 21 S. L. Vega, M. Y. Kwon, K. H. Song, C. Wang, R. L. Mauck, L. Han and J. A. Burdick, *Nat. Commun.*, 2018, **9**, 614.
- 22 W. M. Gramlich, I. L. Kim and J. A. Burdick, *Biomaterials*, 2013, **34**, 9803–9811.
- 23 Z. Pan, Y. Men, S. Senapati and H.-C. Chang, *Biomicrofluidics*, 2018, **12**, 044113.
- 24 Z. Pan and H.-C. Chang, *Phys. Rev. Fluids*, 2019, **4**, 101701.
- 25 D. Hanjaya-Putra, V. Bose, Y.-I. Shen, J. Yee, S. Khetan, K. Fox-Talbot, C. Steenbergen, J. A. Burdick and S. Gerecht, *Blood*, 2011, **118**, 804–815.
- 26 S. Utech, R. Prodanovic, A. S. Mao, R. Ostafe, D. J. Mooney and D. A. Weitz, *Adv. Healthcare Mater.*, 2015, **4**, 1628–1633.
- 27 D. Hanjaya-Putra, J. Yee, D. Ceci, R. Truitt, D. Yee and S. Gerecht, *J. Cell. Mol. Med.*, 2010, **14**, 2436–2447.
- 28 L. Alderfer, E. Russo, A. Archilla, B. Coe and D. Hanjaya-Putra, *FASEB J.*, 2021, e21498.
- 29 T. G. Ingram, *Proc. R. Soc. London, Ser. A*, 1964, **280**, 383–397.
- 30 S. N. Jayasinghe, A. N. Qureshi and P. A. M. Eagles, *Small*, 2006, **2**, 216–219.
- 31 A. Abeyewickreme, A. Kwok, J. R. McEwan and S. N. Jayasinghe, *Integr. Biol.*, 2009, **1**, 260–266.
- 32 S. Zhao, P. Agarwal, W. Rao, H. Huang, R. Zhang, Z. Liu, J. Yu, N. Weisleder, W. Zhang and X. He, *Integr. Biol.*, 2014, **6**, 874–884.
- 33 A. M. Gañán-calvo, J. M. López-herrera, M. A. Herrada, A. Ramos and J. M. Montanero, *J. Aerosol Sci.*, 2018, **125**, 32–56.
- 34 N. Chetwani, S. Maheshwari and H.-C. Chang, *Phys. Rev. Lett.*, 2008, **101**, 204501.
- 35 J. E. Gordon, Z. Gagnon and H.-C. Chang, *Biomicrofluidics*, 2007, **1**, 044102.
- 36 S. Maheshwari and H.-C. Chang, *Appl. Phys. Lett.*, 2006, **89**, 234103.
- 37 S. Maheshwari and H.-C. Chang, *J. Appl. Phys.*, 2007, **102**, 034902.
- 38 E. Ward, E. Chan, K. Gustafsson and S. N. Jayasinghe, *Analyst*, 2010, **135**, 1042.
- 39 D. Hanjaya-Putra, K. T. Wong, K. Hirotsu, S. Khetan, J. A. Burdick and S. Gerecht, *Biomaterials*, 2012, **33**, 6123–6131.
- 40 B. Xia, K. Krutkramelis and J. Oakey, *Biomacromolecules*, 2016, **17**, 2459–2465.
- 41 S. Gerecht, J. A. Burdick, L. S. Ferreira, S. A. Townsend, R. Langer and G. Vunjak-Novakovic, *Proc. Natl. Acad. Sci. U. S. A.*, 2007, **104**, 11298–11303.
- 42 K. J. Wolf and S. Kumar, *ACS Biomater. Sci. Eng.*, 2019, **5**, 3753–3765.
- 43 J. A. Burdick and G. D. Prestwich, *Adv. Mater.*, 2011, **23**, H41–H56.
- 44 S. Khetan, M. Guvendiren, W. R. Legant, D. M. Cohen, C. S. Chen and J. A. Burdick, *Nat. Mater.*, 2013, **12**, 458–465.
- 45 M. Guvendiren and J. A. Burdick, *Nat. Commun.*, 2012, **3**, 792.
- 46 L. Zou, A. S. Braegelman and M. J. Webber, *ACS Appl. Mater. Interfaces*, 2019, **11**, 5695–5700.
- 47 S. Khetan, J. S. Katz and J. A. Burdick, *Soft Matter*, 2009, **5**, 1601–1606.
- 48 O. Chaudhuri, L. Gu, D. Klumpers, M. Darnell, S. A. Bencherif, J. C. Weaver, N. Huebsch, H. P. Lee, E. Lippens, G. N. Duda and D. J. Mooney, *Nat. Mater.*, 2016, **15**, 326–+.
- 49 C. B. Highley, K. H. Song, A. C. Daly and J. A. Burdick, *Adv. Sci.*, 2018, **6**, 1801076.
- 50 M. A. Skylar-Scott, S. G. M. Uzel, L. L. Nam, J. H. Ahrens, R. L. Truby, S. Damaraju and J. A. Lewis, *Sci. Adv.*, 2019, **5**, eaaw2459.
- 51 A. Lee, A. R. Hudson, D. J. Shiwerski, J. W. Tashman, T. J. Hinton, S. Yerneni, J. M. Bliley, P. G. Campbell and A. W. Feinberg, *Science*, 2019, **365**, 482–487.
- 52 D. R. Griffin, M. M. Archang, C.-H. Kuan, W. M. Weaver, J. S. Weinstein, A. C. Feng, A. Ruccia, E. Sideris, V. Ragkousis, J. Koh, M. V. Plikus, D. Di Carlo, T. Segura and P. O. Scumpia, *Nat. Mater.*, 2020, 1–10.
- 53 N. J. Darling, W. Xi, E. Sideris, A. R. Anderson, C. Pong, S. T. Carmichael and T. Segura, *Adv. Healthcare Mater.*, 2020, **9**, 1901391.
- 54 V. G. Muir, T. H. Qazi, J. Shan, J. Groll and J. A. Burdick, *ACS Biomater. Sci. Eng.*, 2021, DOI: 10.1021/acsbiomaterials.0c01612.
- 55 D. Hanjaya-Putra, K. T. Wong, K. Hirotsu, S. Khetan, J. A. Burdick and S. Gerecht, *Biomaterials*, 2012, **33**, 6123–6131.
- 56 E. Hui, K. I. Gimeno, G. Guan and S. R. Caliari, *Biomacromolecules*, 2019, **20**, 4126–4134.
- 57 Z. Wei, R. Schnellmann, H. C. Pruitt and S. Gerecht, *Cell Stem Cell*, 2020, **27**, 798–812.e6.
- 58 H. Qazi and J. A. Burdick, *Biomaterials and Biosystems*, 2021, **1**, 100008.